ACS APPLIED MATERIALS & INTERFACES

Research Article

www.acsami.org

Microwave-Assisted Synthesis of Wavelength-Tunable Photoluminescent Carbon Nanodots and Their Potential Applications

Hongying Liu,[†,‡] Zhimei He,[†] Li-Ping Jiang,*[,†] and Jun-Jie Zhu*[,†]

[†]State Key Laboratory of Analytical Chemistry for Life Science, School of Chemistry & Chemical Engineering, Nanjing University, Nanjing 210093, People's Republic of China

[‡]College of Life Information Science & Instrument Engineering, Hangzhou Dianzi University, Hangzhou 310018, People's Republic of China

Supporting Information

ABSTRACT: A facile and rapid strategy was developed for the synthesis of ultrabright luminescent carbon nanodots (CDs) with tunable wavelength from 464 to 556 nm by introducing glutaraldehyde into the precursor solution under microwave irradiation. The fluorescence properties, including excitation and emission wavelength, quantum yield, and size of the CDs, were adjusted by changing the amount of glutaraldehyde and poly(ethylenimine). Several methods such as high-resolution transmission electron microscopy, X-ray photoelectron spectroscopy, and dynamic light scattering, UV−vis, fluorescence, and Fourier transform infrared spectroscopy were employed to study the morphology and the properties of CDs. The luminescence mechanism was also discussed. In addition, confocal microscopy imaging revealed that the as-prepared CDs could be used as effective fluorescent probes in the cell imaging without obvious cytotoxicity. Moreover, a novel sensor for the detection of Co^{2+} was proposed on the basis of Co^{2+}-induced fluorescence quenching. These superior properties demonstrated the potential application of the CDs in cellular imaging and ion sensing.

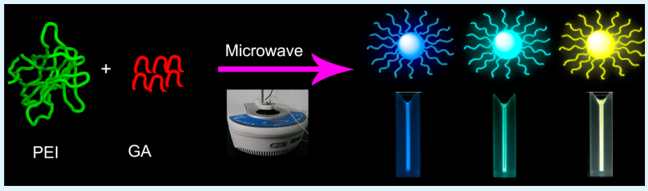

KEYWORDS: *microwave, carbon nanodots, wavelength-tunable, imaging, Co^{2+}*

1. INTRODUCTION

Carbon nanodots (CDs) represent a novel species of zero-dimension carbon nanomaterials of nearly spherical geometry.[1] As a rising star in the field of luminescent nanomaterials, CDs have attracted increasing attention due to their appealing properties, for instance, bright luminescence, good solubility, high chemical inertness, excellent biocompatibility, easy functionalization, and low toxicity.[2−6] These superior features make CDs promising alternative probes for bioimaging and bioassay.[7−12] So far, various methods have been explored to prepare CDs, including arc discharge,[13] laser ablation of graphite,[14] electrochemical synthesis,[15] chemical oxidation,[16] supported synthesis,[17] ultrasonic methods,[18,19] and thermal oxidation.[20] However, most of these methods may involve an expensive carbon source, complex reactions, time-consuming processes, and post-treatment procedures, which limit the applications. Thus, simple, environmentally viable, and sustainable synthetic routes for large-scale production of high-quality fluorescent CDs are in high demand. Moreover, tunable photoluminescence (PL) emissions and substantially high quantum yields (QY) are required in order to ensure good performance in light emitting diodes and bioimaging applications. Therefore, it is potentially promising to explore alternative approaches to synthesize CDs with tunable emission. Nevertheless, to the best of our knowledge, efficient strategies for acquiring CDs with tunable emission are still scarce and highly worthy.

Microwave-assisted technique was an effective route for gaining nanoparticles.[21−24] It provides rapid and uniform heating to the reaction medium, thereby dramatically shortening the reaction time and greatly improving the product yield and purity.[25−27] Compared to conventional methods, the microwave-assisted approach shows many distinct advantages in the preparation of nanoparticles, such as nonhazardous, controllable conditions and rapid reaction rate. Because of such versatility, it is desirable to explore the microwave approach as a promising synthetic route of high-quality luminescent CDs with tunable fluorescence emission wavelength.

Poly(ethylenimine) (PEI) is a harmless, sterile, and biocompatible cationic polymer containing several amino groups in its molecular structure.[28] Consequently, the use of PEI as a precursor can induce the production of nanoparticles with functional amino groups. Meanwhile, glutaraldehyde has been widely applied in biological area as cross-linker due to its high activity.[29,30] Through aldehyde−ammonia condensation reaction of the aldehyde groups with the $-NH_2$ of PEI, the

Received: December 20, 2014
Accepted: February 11, 2015
Published: February 11, 2015

DOI: 10.1021/am508994w
ACS Appl. Mater. Interfaces 2015, 7, 4913−4920

precursors with various content of oxygen can be obtained. This provides promising potential to get fluorescent CDs with tunable wavelength under microwave irradiation.

Herein, a facile, rapid and one-pot microwave-assisted green synthetic approach was explored to synthesize blue luminescent CDs (B-CDs). The introduction of glutaraldehyde into the reaction solution was used to control the fluorescence properties of CDs. By means of varying the initial molar ratio of glutaraldehyde to PEI, we prepared luminescent CDs (T-CDs) with tunable color from blue to yellow (wavelength, 464−556 nm). Furthermore, yellow luminescent CDs (Y-CDs) were used for cellular imaging on the basis of their good biocompatibility and excellent cytocompatibility. Besides, it was also found that Co^{2+} selectively quenched the fluorescence of B-CDs.

2. EXPERIMENTAL SECTION

2.1. Chemicals and Materials. Glutaraldehyde (25% in H_2O) and PEI were purchased from Sigma-Aldrich (Beijing, China) and Shanghai Reagent Co. (Shanghai, China), respectively. Dulbecco's modified Eagle's medium (DMEM), 3-(4,5-dimethylthiazol-2-yl)-2,5-diphenyltetrazolium bromide (MTT), and fetal bovine serum were purchased from Nanjing KeyGen Biotech Co. Ltd. (Nanjing, China).

2.2. Apparatus. The UV−vis absorption spectra were acquired with a Shimadzu 3600 UV−vis spectrometer (Shimadzu, Japan). The fluorescence measurement and lifetime was carried out using a NF920 fluorescence spectrometer (Edinburgh). The high-resolution transmission electron microscopy (HRTEM) images were recorded with a JEOL JSM-6340F microscope. X-ray photoelectron spectroscopy (XPS) was obtained from an ESCALAB MK II X-ray photoelectron spectrometer. Fourier transform infrared (FTIR) spectroscopic measurements were conducted on a Bruker model VECTOR22 spectrometer. Atomic force microscopy (AFM) was performed on an SPI3800 controller (the acquisition frequency and line density were 1.5 Hz and 512.2 × 2 μm scans, respectively). Dynamic light scattering (DLS) experiments were implemented in water at room temperature with a 90Plus particle size analyzer from Brookhaven Instruments Corp. MTT assay was determined by Bio-Rad 680 microplate reader (Philadelphia, PA). Leica TCS SP5 was used to study the confocal scanning microscopy experiments.

2.3. Synthesis of B-CDs and T-CDs. In a typical synthesis, PEI aqueous solution (20 mL, 5 mg mL^{-1}) was stirred vigorously and then transferred into the CEM Instruments (CEM Discover synthesis system, Matthews, NC). The reaction was carried out under microwave irradiation (200 W) at 180 °C. High-quality B-CDs were obtained after 15 min. For the preparation of T-CDs, 0−800 μL of glutaraldehyde was added to the freshly prepared PEI aqueous solution (20 mL, 5 mg mL^{-1}). The mixture was first stirred vigorously in order to turn it into a transparent homogeneous solution, and then it was transferred into the CEM instruments at controlled reaction temperature of 180 °C for 0.5 h. The final product solution of B-CDs and T-CDs was obtained by dialyzing for 5 days using a dialysis bag with 1000 Da molecular weight.

2.4. Quantum Yield Calculations. QY was calculated by counting the integrated PL intensities (excited at 340 nm) and the absorbance value (at 340 nm) of CDs using quinine sulfate as a reference.[31] Quinine sulfate was dissolved in 0.1 M H_2SO_4 (QY 54%). The absorption of samples was kept below 0.1. The quantum yield was calculated by the following equation:

$$\phi_{CDs} = \phi_{ST}\left(\frac{F_{CDs}}{F_{ST}}\right)\left(\frac{A_{ST}}{A_{CDs}}\right)\left(\frac{\eta_{CDs}}{\eta_{ST}}\right)^2$$

where the subscripts CDs and ST stand for carbon nanodots and quinine sulfate, respectively, ϕ is QY, A is the absorbance, and I is the refractive index of the solvent.

2.5. Cell Culture and Confocal Microscopy Imaging. Human cervical carcinoma HeLa cells were maintained in DMEM medium including 10% fetal calf serum, 100 μg mL^{-1} penicillin, and 100 μg mL^{-1} streptomycin at 5% CO_2 and 37 °C. The cells were seeded onto a well plate for 24 h after the concentration reached 5 × 10^5 cells mL^{-1}. Then, the cells were incubated with 100 μg mL^{-1} CDs for 2 h and then washed with phosphate buffer solution (PBS) three times. Finally, the imaging experiments were conducted (20× objective).

2.6. Cytotoxicity Assay. The cytotoxicity was calculated by MTT assay on HeLa cells.[32] First, HeLa cells were seeded in 96-well plates at 5 × 10^3 cells/well. After 12 h, they were seeded with medium including different concentrations of B-CDs and T-CDs (0, 10, 20, 50, 100, 200, and 400 μg mL^{-1}). Twenty-four hours later, 10 μL of MTT (5 mg mL^{-1}) was added and incubated for another 4 h. Then, the medium was removed and 100 μL of DMSO were added. The absorbance of each well was collected. The cytotoxicity was calculated by the following equation:

$$\text{cell viability (\%)} = A_1/A_2 \times 100$$

where A_1 is the absorbance of the well in which the cells were exposed to the CDs, while A_2 is the absorbance of the well in which the cells were not exposed to the CDs. Six replicate wells were used for each control and test concentration per well. Results are presented with their standard deviations.

3. RESULTS AND DISCUSSION

3.1. Synthesis of the CDs. The synthetic pathway of the CDs is illustrated in Scheme 1. The fluorescent B-CDs were prepared in PEI solution under microwave irradiation within 15 min. The fluorescence intensity of B-CDs is influenced by the concentration of PEI, reaction temperature, and irradiation time. Thus, the evolution of quantum yield was studied to optimize experimental parameter. We optimize the PEI concentration first. The experimental data showed that a considerable increase of QY with the concentration of PEI between 0.5 and 5.0 mg mL^{-1} was obtained (Figure 1a). The reason is that the nucleus of carbon nanodots increased as the concentration of PEI increased. Hydrogen atoms of PEI molecules could react with hydroxyl groups of water. Moderate PEI could speed up the dehydration reaction. After that, QY decreased because overmuch PEI could dilute the concentration of water, which results in an incomplete reaction. Furthermore, the dynamic viscosity of PEI solution increased as the concentration of PEI increased. Extra viscosity will hinder the formation of carbon nanodots. As a result, 5.0 mg mL^{-1} of PEI was chosen. The effect of reaction temperature on QY is also exhibited in Figure 1b. A significant increase of QY was obtained between 100 and 180 °C. Conversely, when the temperature increased from 180 to 200 °C, we could not find a substantial enhancement of the QY. Besides, the influence of the reaction time on QY was investigated. As shown in Figure 1c, QY gradually increased with increasing irradiation time and starts to level off after 15 min. Furthermore, at the beginning, the solution is colorless, and no absorption is observed. After microwave irradiation, a maximal absorption peak at 360 nm of the solution could be observed. The absorption intensity increased with increasing irradiation time. As a result, 15 min

Scheme 1. Schematic Illustration of the Synthetic Pathway

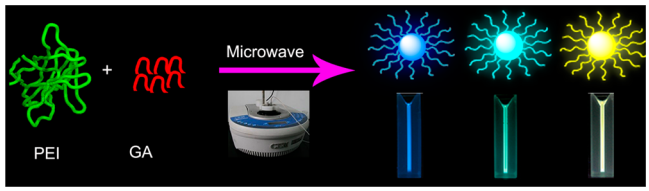

DOI: 10.1021/am508994w
ACS Appl. Mater. Interfaces 2015, 7, 4913−4920

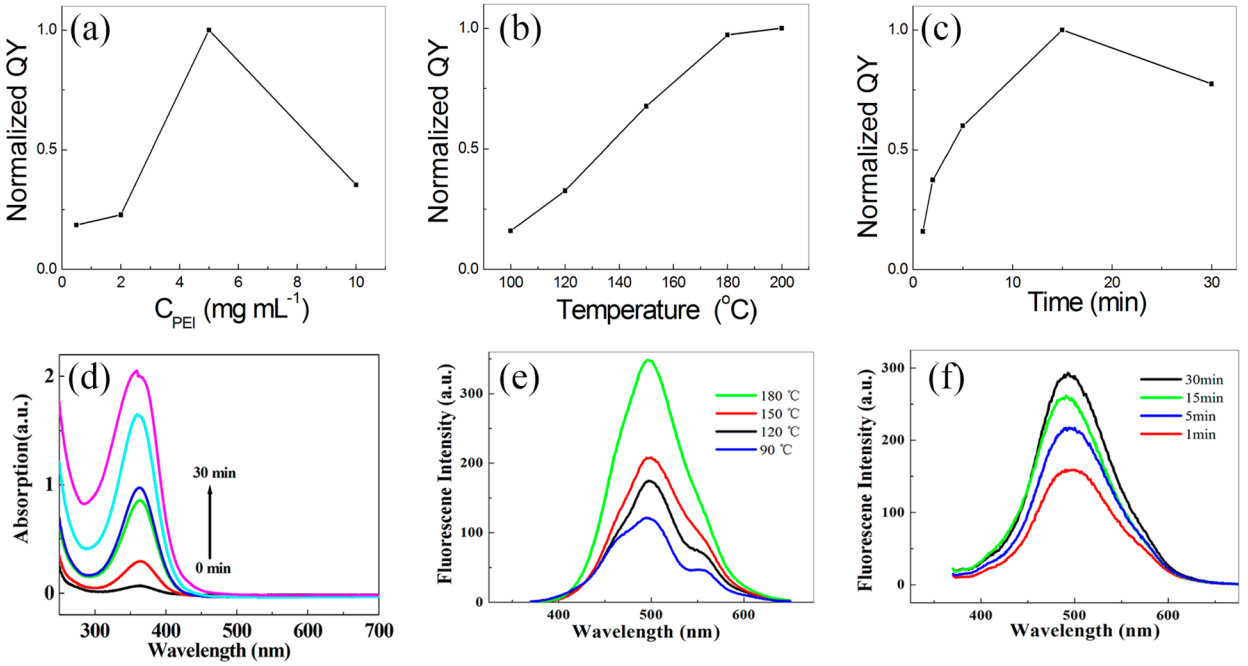

Figure 1. Effects of (a) concentration of PEI, (b) reaction temperature, and (c) reaction time on the normalized quantum yield. (d) UV−vis spectra of B-CDs with the duration of microwave irradiation. (e) Fluorescence spectra of T-CDs from samples with different reaction temperature. (f) Fluorescence emission spectra of T-CDs from samples with different irradiation time.

was selected as the optimal reaction time. To confirm the effect of microwave irradiation on the reaction rate, we compared the emission of B-CDs prepared by hydrothermal route and microwave method. The experimental data exhibited that the fluorescence intensity of B-CDs with hydrothermal route was 2.1 times lower than that of microwave method. Furthermore, the T-CDs with tunable color from blue to yellow were observed by adopting glutaraldehyde as cross-linking reagent, as shown in Scheme 1. Similarly, we studied reaction temperature and reaction time to find the optimal synthesis conditions for T-CDs. In Figure 1e,f, the optimal temperature and microwave irradiation time are 180 °C and 30 min, respectively. Clearly, microwave irradiation could shorten the reaction time and simplify the synthetic procedure enormously, while the fluorescence properties are tuned by the introduction of glutaraldehyde.

3.2. Optical Characterization. The optical properties of B-CDs and T-CDs were explored by PL and UV−vis spectra (Figure 2). The B-CDs aqueous solution exhibits blue fluorescence under UV lamp (Figure 2a), and a typical absorption peak at 360 nm (Figure 2c). The B-CDs also display an excitation-dependency PL behavior. The PL peak of B-CDs shifts to longer wavelength with the excitation wavelength ranging from 300 to 520 nm. The PL spectrum also exhibits that the optimal emission wavelength is 464 nm while the excitation is at 347 nm. Two distinct excitation peaks appeared at 347 and 265 nm (Figure 2b), which correspond to 360 nm absorption band of B-CDs and the strong background adsorption from $\pi-\pi^*$ transition, respectively. After glutaraldehyde was added into the reaction solution, the fluorescence properties of the CDs, such as emission wavelength and QY, changed. With different molar ratios of glutaraldehyde to PEI, T-CDs were prepared with tunable wavelength ranging from 464 to 556 nm and color varying from blue to yellow (Figure 2a,f). A typical CD sample (Y-CDs) was studied to explore the optical properties of CDs following the addition of glutaraldehyde. As shown in Figure 2a, the Y-CD aqueous solution exhibits yellow fluorescence under UV lamp. The PL spectra of Y-CDs also show a similar wavelength excitation-dependency feature. The PL peaks shift to longer wavelength, and the excitation wavelength increases from 340 to 520 nm. The optimized emission and excitation peak is at 520 and 358 nm. The PL excitation spectra show tiny differences: a red-shifted peak at 358 nm can be observed in Figure 2b. In addition, the QY values of B-CDs and Y-CDs were found to be 10 and 8%, respectively, which were calculated using quinine sulfate as a reference.[11] The fluorescence lifetime of B-CDs and Y-CDs was also studied. All the fluorescence emissions exhibited well fitted biexponential functions, as shown in Figure 2 and Figure S2 Supporting Information. The observed lifetimes of B-CDs and Y-CDs are summarized in Table 1. The lifetime of B-CDs increased from the initial value of 5.7 to 8.4 μs after the addition of glutaraldehyde. As far as we know, this is the longest lifetime reported ever for CDs.

3.3. Structural Characterization. The size of nanoparticles is important for bioapplications. On one hand, it should be large enough to deny rapid leakage into blood capillaries. On the other hand, it should be small enough to escape capture by fixed macrophages lodging in the reticuloendothelial system.[33] To characterize the morphology and the size of the CDs, we used HRTEM, DLS, and AFM. In Figure 3a,b, the CDs show high crystallinity and monodispersity. The distribution of the B-CDs diameter ranges from 2 to 7 nm, with an average size of 5 nm. After the addition of glutaraldehyde, the average size of Y-CDs increases to 10 nm. Furthermore, representative AFM images of B-CDs and Y-CDs are shown in Figure 3c,d. The particle size observed in AFM images is consistent with that obtained through analysis of HRTEM micrographs. However, the corresponding hydrodynamic diameter of B-CDs and Y-CDs measured by DLS is equal to 10 and 15 nm, respectively, which is larger than that

DOI: 10.1021/am508994w
ACS Appl. Mater. Interfaces 2015, 7, 4913−4920

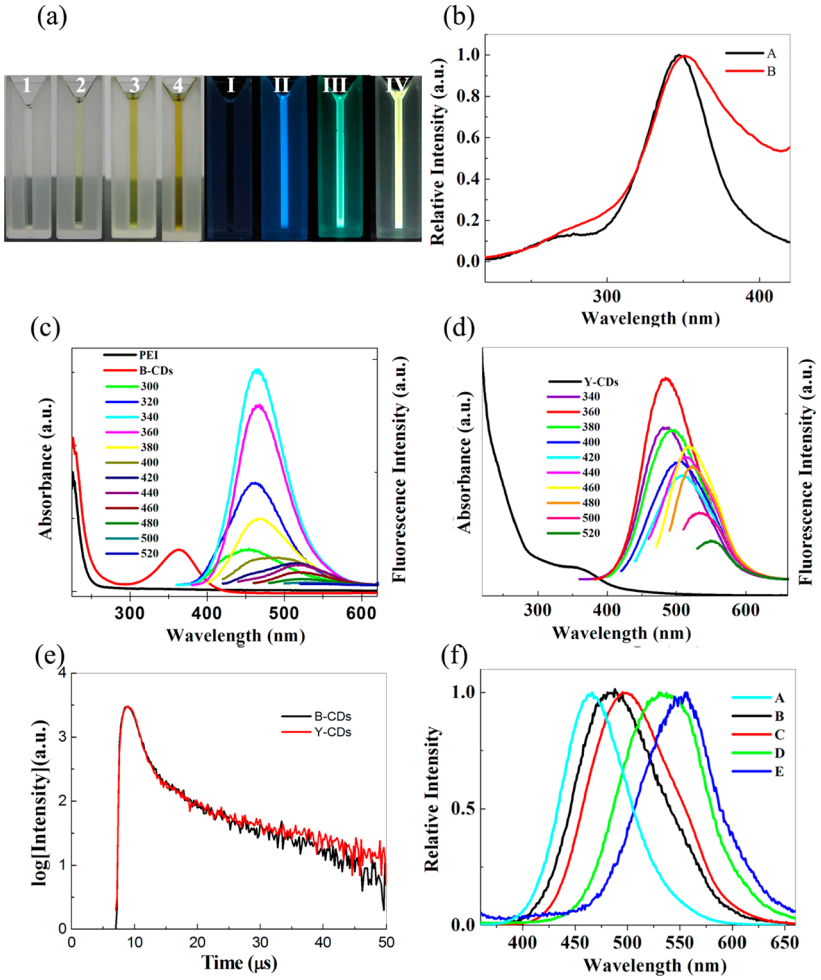

Figure 2. (a) Photographs of the (1, I) PEI, (2, II) B-CDs, and (3, 4 and III, IV) T-CDs solution under (left) visible light and (right) UV light. (b) PL excitation spectra of (A) B-CDs and (B) Y-CDs. (c) UV−vis spectrum of (black) PEI and (red) B-CDs, and the excitation-dependent PL behaviors. (d) UV−vis spectrum of Y-CDs and the excitation-dependent PL behaviors. (e) Time-resolved fluorescence decay of (black) B-CDs and (red) Y-CDs. (f) Normalized PL spectra of T-CDs prepared at various volumes of glutaraldehyde: (A) 0, (B) 100, (C) 200, (D) 400, and (E) 800 μL.

Table 1. Fluorescence Lifetime of the B-CDs and Y-CDs

	τ_1 (μs)	τ_2 (μs)	av τ (μs)	Chi
B-CDs	1.28	11.5	5.7	1.486
Y-CDs	1.17	14.29	8.4	1.783

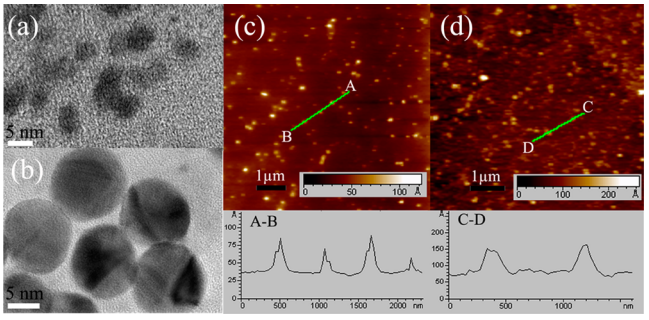

Figure 3. HRTEM images of (a) B-CDs and (b) Y-CDs. AFM images of (c) B-CDs and (d) Y-CDs.

found through TEM and AFM analysis, due to the hydration effects present in aqueous solution. This discrepancy may be explained by the fact that the polymer chains surround the core. The diameter of the CDs was measured by TEM and AFM after they were dried on the surface, while DLS was used to determine the diameter of CDs in aqueous solution when they were hydrated and consequently in a more "swollen" state. Thus, the size of CDs is suitable for biological systems.

Furthermore, FTIR experiments were carried out to identify functional groups modified on the surface of CDs.[34,35] As shown in Figure 4a,b, the CDs show a new peak at 1645 cm^{-1} and three strong peaks at 1570, 1472, and 1309 cm^{-1}, which correspond to C═O, N−H, CH_2, and C−N, respectively. The broad band at 3360−2500 cm^{-1} indicates the presence of −OH and N−H. The difference between PEI and CDs is the absorption at 1645 and 1570 cm^{-1}. The above results demonstrate that polymer chains were retained on the CDs. Furthermore, XPS was used to analyze the surface composition and the structure of the CDs. The spectra of B-CDs and Y-CDs show three peaks at 284.0, 400.0, and 530.6 eV, which correspond with C_{1s}, N_{1s}, and O_{1s}, respectively[36] (Figure 4c). The O peak of B-CDs may come from H_2O, O_2, or CO_2 adsorbed on the surfaces of CDs, and the XPS chamber. The oxygen content of CDs increases after the glutaraldehyde is introduced, and such increase coincides with the red-shifted emission of CDs. High-resolution XPS spectra of C_{1s} for B-CDs

DOI: 10.1021/am508994w
ACS Appl. Mater. Interfaces 2015, 7, 4913−4920

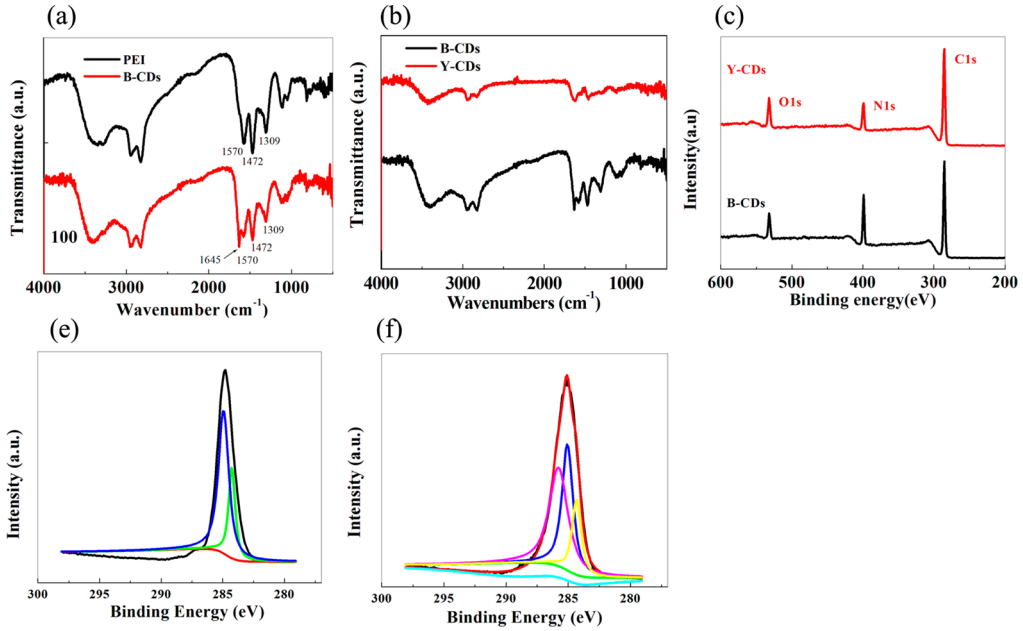

Figure 4. FTIR spectra of (a) PEI, B-CDs and (b) Y-CDs. (c) XPS spectra of B-CDs and Y-CDs. C_{1s} high-resolution XPS spectra of (e) B-CDs and (f) Y-CDs.

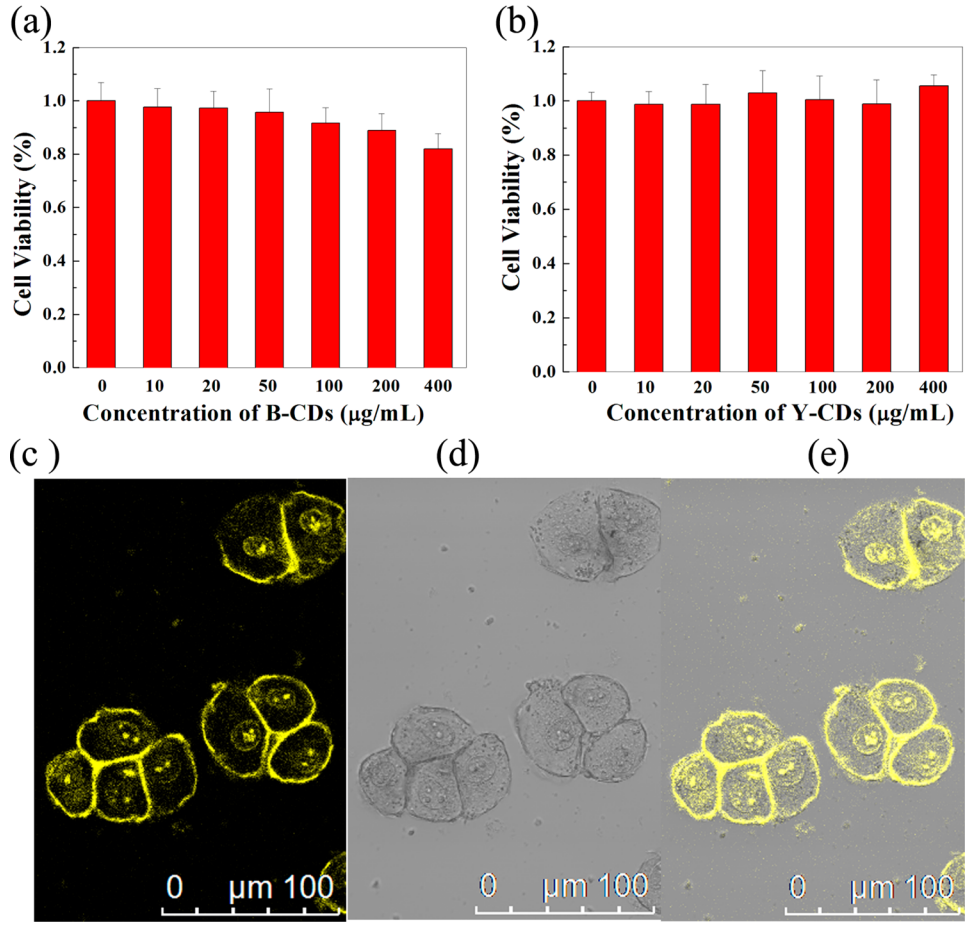

Figure 5. Cell viability of (a) B-CDs and (b) Y-CDs with different concentrations and incubation with HeLa cells for 24 h. (c) Confocal fluorescence, (d) bright-field, and (e) merged images of the HeLa cells after 2 h incubation with Y-CDs.

and Y-CDs are also shown in Figure 4e,f. The C_{1s} spectrum of Y-CDs shows four peaks at 284.3, 285.0, 285.8, and 288.6 eV, which are attributed to C−C, C−N, C−O, and C═O, respectively. Because the experimental data demonstrate that the oxygen-related states on CDs increased with further oxidation, the red-shift of the CD emission comes from

DOI: 10.1021/am508994w
ACS Appl. Mater. Interfaces 2015, 7, 4913−4920

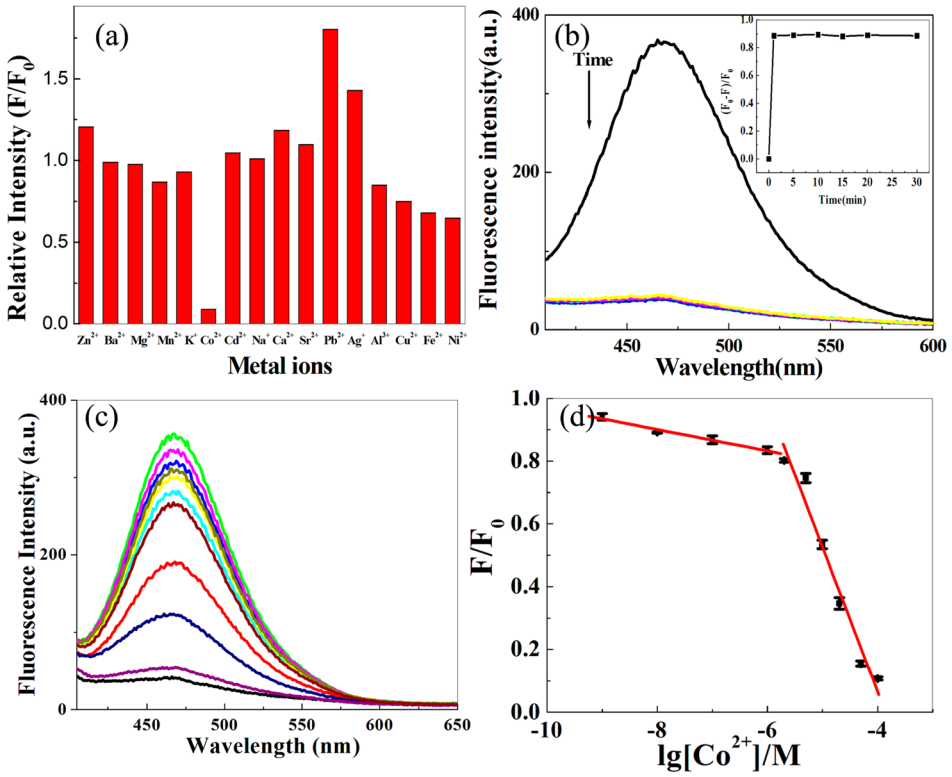

Figure 6. (a) Fluorescence responses of B-CDs to 16 metal ions (1 mM). (b) Time-dependent fluorescence response of the B-CDs to 0.5 mM Co^{2+}; (inset) plot of $(F - F_0)/F_0$ versus time in the presence of 0.5 mM Co^{2+}. (c) Fluorescence emission spectra of B-CDs in the presence of different concentrations of Co^{2+}. (d) Relationship between the fluorescence intensity of B-CDs and the logarithmic concentration of Co^{2+}.

oxygen-related states instead of size effect.[37] The behavior of CDs after oxidation was the same as that of silicon nanocrystals. For silicon nanocrystals, the red-shift fluorescence comes from the surface state of silanone and siloxane groups; the higher the surface oxidation, the greater the amount of surface defects. These defects can trap excitons, resulting in a red-shift of the emission wavelength.

3.4. Cell Imaging. First of all, the use of CDs in cell imaging was investigated. In order to explore the application of B-CDs and Y-CDs in biolabeling, some preliminary tests were carried out. As it is important to test the stability of B-CDs and Y-CDs under physiological conditions, the influence of pH on the fluorescence intensity was investigated (Figure S3A, Supporting Information). The PL intensity of B-CDs decreases with the increase of the pH value. Yet, the intensity is enough to make them attractive for biorelated applications. The maximum intensity of Y-CDs is obtained at pH 7.4 (Figure S4A, Supporting Information). Besides, B-CDs and Y-CDs show ionic strength-resistant optical properties. This is superior to other CDs reported previously because of their ionic strength-dependent optical properties.[38,39] Furthermore, these CDs were stable for one month in aqueous solution with no decrease in optical performance. All of these results indicate that B-CDs and Y-CDs possess high stability. Additionally, the photostability of B-CDs and Y-CDs was also studied. As shown in Figures S3C and S4C (Supporting Information), upon extended UV irradiation, the PL intensity is decreases as a result of the degradation of the retained polymer chains. The cytotoxicity of B-CDs and Y-CDs was evaluated with MTT viability assay. Figure 5a,b shows the cell viability after incubation with B-CDs and Y-CDs at concentrations of 10, 20, 50, 100, 200, and 400 $\mu g\ mL^{-1}$ for 24 h. It is worth noting that both of them possess low cytotoxicity even at 200 $\mu g\ mL^{-1}$ after 24 h. Moreover, the cytotoxicity of Y-CDs is lower than that of B-CDs. This means that the CDs have better biocompatibility after incorporating glutaraldehyde by cross-linking strategy. Thus, Y-CDs show more potential for single molecular imaging and tracking in living cells. To explore this application, we studied confocal fluorescence images. In Figure 5c, a bright yellow area inside HeLa cells can be seen, indicating successful translocation of Y-CDs through the cell membrane and effective labeling on the cell membrane and nucleus. These preliminary results demonstrate that Y-CDs are suitable candidates for cell imaging, biosensing, and drug delivery.

3.5. Detection of Co^{2+}. Cobalt is an essential element of the organism, and its toxicological effects include vasodilatation, flushing, and cardiomyopathy in humans and animals.[40] As a consequence, selective monitoring of Co^{2+} in environmental and food samples is particularly sought after. Conventional metal-based quantum dots have been successfully used as optical probe in this type of assay.[41] However, the toxicity of heavy metal elements limited their application. For this reason, it is highly demanded to find nontoxic nanomaterials for Co^{2+} sensing. Due to their excellent fluorescence properties, B-CDs were adopted in this application.

To explore the suitability of B-CDs, fluorescence intensity of B-CDs solutions was studied in the presence and absence of Co^{2+}. B-CDs exhibited strong fluorescence in the absence of metal ions, while the existence of Co^{2+} led to a significant decrease of fluorescence intensity. This phenomenon shows that B-CDs could be used to detect Co^{2+}. Considering the physiological buffer system, pH 7.4 was taken. Lower concentrations of fluorescent probe showed higher sensitivity, while higher concentrations exhibited a broader detection

DOI: 10.1021/am508994w
ACS Appl. Mater. Interfaces 2015, 7, 4913−4920

range. Hence, the concentration of B-CDs was optimized. The results showed that the optimal concentration of B-CDs is 400 nM.

The selectivity of the proposed system was evaluated by determining the PL intensity in the presence of metal ions including Zn^{2+}, Ba^{2+}, Mg^{2+}, Mn^{2+}, K^{+}, Cd^{2+}, Na^{+}, Ca^{2+}, Sr^{2+}, and Pb^{2+}. As shown in Figure 6a, the fluorescence of B-CDs was almost completely quenched upon the addition of Co^{2+}. In contrast, no obvious decrease was obtained after adding other ions. Thus, this system has high selectivity toward Co^{2+}. Furthermore, the relationship between PL intensity and time was also studied, as shown in Figure 6b. The fluorescence intensity was completely quenched within 1 min, indicating that this sensing system responds rapidly. Next, we also evaluate the sensitivity by monitoring the PL intensity upon adding Co^{2+} for 1 min. As shown in Figure 6c, the PL intensity of B-CDs gradually decreases with increasing the concentration of Co^{2+}. Two good linear relationships exist between the PL intensity of B-CDs and the logarithm of the concentration of Co^{2+} ranging from 1 nM to 100 μM. The detection limit is 0.3 nM, with the signal-to-noise ratio (S/N) equal to 3.

4. CONCLUSION

Herein, CDs were synthesized by a microwave-assisted method. For this tunable fluorescence system, glutaraldehyde was adopted as cross-linking reagent. The fluorescence emissions of CDs were adjusted in the wavelength range of 464−556 nm, depending on the amount of glutaraldehyde. The synthesized CDs show excellent fluorescence properties, low toxicity, good stability, and water solubility. Hence, this method is simple, easily controllable, and readily scalable to an industrial level. Furthermore, the fluorescent CDs can be used as fluorescence probes for cell imaging and Co^{2+} sensing. Therefore, the obtained CDs are promising for applications in biosensing and cell imaging in the future.

■ ASSOCIATED CONTENT

Supporting Information

Fluorescence emission spectra of B-CDs from samples with different molecule weight of PEI and the stability of B-CDs and Y-CDs under physiological conditions. This material is available free of charge via the Internet at http://pubs.acs.org.

■ AUTHOR INFORMATION

Corresponding Authors

*E-mail: jjzhu@nju.edu.cn. Tel./Fax: +86-25-83597204.
*E-mail: Jianglp@nju.edu.cn.

Notes

The authors declare no competing financial interest.

■ ACKNOWLEDGMENTS

This work is supported by the National Natural Science Foundation of China (Nos. 21121091, 21405029, 21475057), the International S&T Cooperation Projects of China (2010DFA42060), and the State Key Laboratory of Analytical Chemistry for Life Science (SKLACLS1305). This work is also supported by the Program for New Century Excellent Talents in University (NCET-12-0256).

■ REFERENCES

(1) Xu, X. Y.; Ray, R.; Gu, Y. L.; Ploehn, H. J.; Gearheart, L.; Raker, K.; Scrivens, W. A. Electrophoretic Analysis and Purification of Fluorescent Single-Walled Carbon Nanotube Fragments. *J. Am. Chem. Soc.* **2004**, *126*, 12736−12737.

(2) Sun, Y. P.; Zhou, B.; Lin, Y.; Wang, W.; Fernando, K. A. S.; Pathak, P.; Meziani, M. J.; Harruff, B. A.; Wang, X.; Wang, H.; Luo, P. G.; Yang, H.; Kose, M. E.; Chen, B.; Veca, L. M.; Xie, S. Y. Quantum-Sized Carbon Dots for Bright and Colorful Photoluminescence. *J. Am. Chem. Soc.* **2006**, *128*, 7756−7757.

(3) Zheng, L.; Chi, Y.; Dong, Y.; Lin, J.; Wang, B. Electrochemiluminescence of Water-Soluble Carbon Nanocrystals Released Electrochemically from Graphite. *J. Am. Chem. Soc.* **2009**, *131*, 4564−4565.

(4) Baker, S. N.; Baker, G. A. Luminescent Carbon Nanodots: Emergent Nanolights. *Angew. Chem., Int. Ed.* **2010**, *49*, 6726−6744.

(5) Li, H. T.; He, X. D.; Kang, Z. H.; Huang, H.; Liu, Y.; Liu, J. L.; Lian, S. Y.; Tsang, C. C. A.; Yang, X. B.; Lee, S. T. Water-Soluble Fluorescent Carbon Quantum Dots and Catalyst Design. *Angew. Chem., Int. Ed.* **2010**, *49*, 4430−4434.

(6) Ma, Z.; Zhang, Y. L.; Wang, L.; Ming, H.; Li, H. T.; Zhang, X.; Wang, F.; Liu, Y.; Kang, Z. H.; Lee, S. T. Bioinspired Photoelectric Conversion System Based on Carbon Quantum Dot Doped Dye−Semiconductor Complex. *ACS Appl. Mater. Interfaces* **2013**, *5*, 5080−5084.

(7) Esteves, J. C. G.; Goncalves, H. M. R. Analytical and Bioanalytical Applications of Carbon Dots. *Trends Anal. Chem.* **2011**, *30*, 1327−1336.

(8) Sanderson, K. Quantum Dots Go Large. *Nature* **2009**, *459*, 760−761.

(9) Cao, L.; Wang, X.; Meziani, J. M.; Lu, F.; Wang, H.; Luo, P. G.; Lin, Y.; Harruff, B. A.; Veca, L. M.; Murray, D.; Xie, S. Y.; Sun, Y. P. Carbon Dots for Multiphoton Bioimaging. *J. Am. Chem. Soc.* **2007**, *129*, 11318−11319.

(10) Yang, S. T.; Cao, L.; Luo, P. G.; Lu, F. S.; Wang, X.; Wang, H. F.; Meziani, M. J.; Liu, Y. F.; Qi, G.; Sun, Y. P. Carbon Dots for Optical Imaging in Vivo. *J. Am. Chem. Soc.* **2009**, *131*, 11308−11309.

(11) Sun, D.; Ban, R.; Zhang, P. H.; Wu, G. H.; Zhang, J. R.; Zhu, J. J. Hair Fiber as a Precursor for Synthesizing of Sulfur- and Nitrogen-Co-doped Carbon Dots with Tunable Luminescence Properties. *Carbon* **2013**, *64*, 424−434.

(12) Li, H. T.; Kang, Z. H.; Liu, Y.; Lee, S. T. Carbon Nanodots: Synthesis, Properties, and Applications. *J. Mater. Chem.* **2012**, *22*, 24230−24253.

(13) Xu, X.; Ray, R.; Gu, Y.; Ploehn, H. J.; Gearheart, L.; Raker, K.; Scrivens, W. A. Electrophoretic Analysis and Purification of Fluorescent Single-Walled Carbon Nanotube Fragments. *J. Am. Chem. Soc.* **2004**, *126*, 12736−12737.

(14) Hu, S. L.; Niu, K. Y.; Sun, J.; Yang, J.; Zhao, N. Q.; Du, X. W. One-Step Synthesis of Fluorescent Carbon Nanoparticles by Laser Irradiation. *J. Mater. Chem.* **2009**, *19*, 484−488.

(15) Zheng, L.; Chi, Y.; Dong, Y.; Lin, J.; Wang, B. Electrochemiluminescence of Water-Soluble Carbon Nanocrystals Released Electrochemically from Graphite. *J. Am. Chem. Soc.* **2009**, *131*, 4564−4565.

(16) Dong, Y.; Pang, H.; Ren, S.; Chen, C.; Chi, Y.; Yu, T. Etching Single-Wall Carbon Nanotubes into Green and Yellow Single-Layer Graphene Quantum Dots. *Carbon* **2013**, *64*, 245−251.

(17) Zong, J.; Yang, X.; Trinchi, A.; Hardin, S.; Cole, I.; Zhu, Y.; Li, C. Z.; Muster, T.; Wei, G. Carbon Dots as Fluorescent Probes for "Off−On" Detection of Cu^{2+} and L-Cysteine in Aqueous Solution. *Biosens. Bioelectron.* **2014**, *51*, 330−335.

(18) Li, H.; He, X.; Liu, Y.; Huang, H.; Lian, S.; Lee, S. T.; Kang, Z. One-Step Ultrasonic Synthesis of Water-Soluble Carbon Nanoparticles with Excellent Photoluminescent Properties. *Carbon* **2011**, *49*, 605−609.

(19) Li, H. T.; He, X. D.; Liu, Y.; Yu, H.; Kang, Z. H.; Lee, S. T. Synthesis of Fluorescent Carbon Nanoparticles Directly from Active Carbon via a One-Step Ultrasonic Treatment. *Mater. Res. Bull.* **2011**, *16*, 147−151.

(20) Dong, Y.; Pang, H.; Yang, H. B.; Guo, C.; Shao, J.; Chi, Y.; Li, C. M.; Yu, T. Carbon-based Dots Co-doped with Nitrogen and Sulfur for

DOI: 10.1021/am508994w
ACS Appl. Mater. Interfaces 2015, 7, 4913−4920

High Quantum Yield and Excitation-Independent Emission. *Angew. Chem., Int. Ed.* **2013**, *52*, 7800−7804.
(21) Zhu, S.; Zhang, J.; Wang, L.; Song, Y.; Zhang, G.; Wang, H.; Yang, B. A General Route to Make Non-Conjugated Linear Polymers Luminescent. *Chem. Commun.* **2012**, *48*, 10889−10891.
(22) Li, L.; Ji, J.; Fei, R.; Wang, C.; Lu, Q.; Zhang, J.; Jiang, L.; Zhu, J. A Facile Microwave Avenue to Electrochemiluminescent Two-Color Graphene Quantum Dots. *Adv. Funct. Mater.* **2012**, *22*, 2971−2979.
(23) Li, L.; Qian, H.; Ren, J. Rapid Synthesis of Highly Luminescent CdTe Nanocrystals in the Aqueous Phase by Microwave Irradiation with Controllable Temperature. *Chem. Commun.* **2005**, *4*, 528−530.
(24) Xiong, W. W.; Yang, G. H.; Wu, X. C.; Zhu, J. J. Aqueous Synthesis of Color-Tunable $CuInS_2$/ZnS Nanocrystals for the Detection of Human Interleukin 6. *ACS Appl. Mater. Interfaces* **2013**, *5*, 8210−8216.
(25) Anumol, E. A.; Kundu, P.; Deshpande, P. A.; Madras, G.; Ravishankar, N. New Insights into Selective Heterogeneous Nucleation of Metal Nanoparticles on Oxides by Microwave-Assisted Reduction: Rapid Synthesis of High-Activity Supported Catalysts. *ACS Nano* **2011**, *5*, 8049−8061.
(26) Liu, S. F.; Lu, F.; Zhu, J. J. Highly Fluorescent Ag Nanoclusters: Microwave-Assisted Green Synthesis and Cr^{3+} Sensing. *Chem. Commun.* **2011**, *47*, 2661−2663.
(27) Roberts, B. A.; Strauss, C. R. Toward Rapid, "Green", Predictable Microwave-Assisted Synthesis. *Acc. Chem. Res.* **2005**, *38*, 653−661.
(28) Liu, C. J.; Zhang, P.; Zhai, X. Y.; Tian, F.; Li, W. C.; Yang, J. H.; Wang, H.; Wang, W.; Liu, W. Nano-Carrier for Gene Delivery and Bioimaging Based on Carbon Dots with PEI-Passivation Enhanced Fluorescence. *Biomaterials* **2012**, *33*, 3604−3613.
(29) Kim, S. Y.; Ramaraj, B.; Yoon, K. R. Preparation and Characterization of Polyvinyl Alcohol-Grafted Fe_3O_4 Magnetic Nanoparticles through Glutaraldehyde. *Surf. Interface Anal.* **2012**, *44*, 1238−1242.
(30) Wang, Q. X.; Zhang, B.; Lin, X. Q.; Weng, W. Hybridization Biosensor Based on the Covalent Immobilization of Probe DNA on Chitosan-Multiwalled Carbon Nanotubes Nanocomposite by Using Glutaraldehyde as an Arm Linker. *Sens. Actuators B* **2011**, *156*, 599−605.
(31) Liu, H. P.; Ye, T.; Mao, C. D. Fluorescent Carbon Nanoparticles Derived from Candle Soot. *Angew. Chem., Int. Ed.* **2007**, *46*, 6473−6475.
(32) Liu, S. H.; Lu, F.; Jia, X. D.; Cheng, F. F.; Jiang, L. P.; Zhu, J. J. Microwave Assisted Synthesis of a Biocompatible Polyacid-Conjugated Fe_3O_4 Superparamagnetic Hybrid. *CrystEngComm* **2011**, *13*, 2425−2429.
(33) Cho, K.; Wang, X.; Nie, S. M.; Chen, Z.; Shin, D. M. Therapeutic Nanoparticles for Drug Delivery in Cancer. *Clin. Cancer Res.* **2008**, *14*, 1310−1316.
(34) Cheng, F.; Zhang, K.; Chen, D.; Zhu, L.; Jiang, M. Self-Assembly of Heteroarms Core-Shell Polymeric Nanoparticles (HCPNs) and Templated Synthesis of Gold Nanoparticles within HCPNs and the Superparticles. *Macromolecules* **2009**, *42*, 7108−7113.
(35) Ogawa, M.; Kataoka, H.; Nitahara, S.; Fujimoto, H.; Aoki, H.; Ito, S.; Narazaki, M.; Matsuda, T. Water-Soluble Fluorinated Polymer Nanoparticle as 19F MRI Contrast Agent Prepared by Living Random Copolymerization from Dendrimer Initiator. *Bull. Chem. Soc. Jpn.* **2012**, *85*, 79−86.
(36) Liu, S.; Tian, J.; Wang, L.; Li, H.; Zhang, Y.; Sun, X. Stable Aqueous Dispersion of Graphene Nanosheets: Noncovalent Functionalization by a Polymeric Reducing Agent and Their Subsequent Decoration with Ag Nanoparticles for Enzymeless Hydrogen Peroxide Detection. *Macromolecules* **2010**, *43*, 10078−10083.
(37) Bao, L.; Zhang, Z. L.; Tian, Z. Q.; Zhang, L.; Liu, C.; Lin, Y.; Qi, B. P.; Pang, D. W. Electrochemical Tuning of Luminescent Carbon Nanodots: From Preparation to Luminescence Mechanism. *Adv. Mater.* **2011**, *23*, 5801−5806.
(38) Chen, L.; Xu, S.; McBranch, D.; Whitten, D. Tuning the Properties of Conjugated Polyelectrolytes through Surfactant Complexation. *J. Am. Chem. Soc.* **2000**, *122*, 9302−9303.
(39) Liu, B.; Wang, S.; Bazan, G. C.; Mikhilovsky, A. Shape-Adaptable Water-Soluble Conjugated Polymers. *J. Am. Chem. Soc.* **2003**, *125*, 13306−13307.
(40) Yuzefovsky, A. I.; Lonardo, R. F.; Wang, M. H.; Michel, R. G. J. Determination of Ultra-Trace Amounts of Cobalt in Ocean Water by Laser-Excited Atomic Fluorescence Spectrometry in a Graphite Electrothermal Atomizer with Semi On-Line Flow Injection Preconcentration. *J. Anal. Atom. Spectrom.* **1994**, *9*, 1195−202.
(41) Chen, J. L.; Zheng, A. F.; Gao, Y. C.; He, C. Y.; Wu, G. H.; Chen, Y. C.; Kai, X.; Zhu, C. Q. Functionalized CdS Quantum Dots-based Luminescence Probe for Detection of Heavy and Transition Metal Ions in Aqueous Solution. *Spectrochim. Acta, Part A* **2008**, *69*, 1044−1052.

DOI: 10.1021/am508994w
ACS Appl. Mater. Interfaces 2015, 7, 4913−4920